Colloidal stability classification of TiO_2 nanoparticles in artificial and in natural waters by cluster analysis and a global stability index: influence of standard and natural colloidal particles

Andrea Brunelli[a], Aurelio Foscari[a], Gianpietro Basei[a,b], Gigliola Lusvardi[c], Cinzia Bettiol[a], Elena Semenzin[a], Antonio Marcomini[a], Elena Badetti[a*]

[a]DAIS - Department of Environmental Sciences, Informatics and Statistics, Ca' Foscari University of Venice, Via Torino 155, 30170 Venice Mestre, Italy

[b]GreenDecision Srl, Via delle industrie 21/8, 30175 Venice, Italy

[c]University of Modena and Reggio Emilia, Via Campi 103, Modena, Italy

*corresponding author: elena.badetti@unive.it

Abstract

The highly complex interactions of engineered nanoparticles (NPs) with natural components in surface waters are considered key factors in understanding the fate and behavior of NPs in the environment. Experimental approaches aiming at imitating environmentally relevant conditions are therefore necessary. In this context, the colloidal behavior of TiO_2 NPs was investigated in both artificial waters and natural brackish water (from the Venice lagoon, Italy), in the presence of standard kaolinite and natural organic matter (NOM), or of the fine fraction of natural colloidal particles (NCPs)

extracted from the lagoon sediment. Both single-component (TiO_2 NPs, kaolinite, kaolinite with NOM addition, and NCPs) and multi-component dispersed phases (TiO_2 NPs/kaolinite, TiO_2 NPs/kaolinite with NOM, and TiO_2 NPs/NCPs) were analyzed by Dynamic and Electrophoretic Light Scattering, as well as by Centrifugal Separation Analysis. The experimental data obtained, i.e. hydrodynamic size, surface charge and sedimentation velocity values, were i) statistically treated by hierarchical clustering and ii) merged into a global stability index (I_G). The hierarchical clustering allowed to group the dispersions into three colloidal stability classes, where the main discriminant was the medium composition (i.e. ionic strength and presence of NOM), while the I_G allowed to establish a colloidal stability ranking of the dispersions within each class. Moreover, the comparison among the different dispersions suggested that kaolinite can be used as a good surrogate for NCPs, to estimate the colloidal behavior and environmental fate of TiO_2 NPs in natural aqueous media.

1. Introduction

The huge benefits of engineered nanoparticles (NPs) in every-day life have led over 5000 consumer nano-based products on the market nowadays, reaching millions of customers (DTU Environment, 2017). An estimation of production volumes indicated that TiO_2 NPs, along with SiO_2 NPs, were the most abundant NPs produced in 2010 with > 10000 t/year, followed by other metal oxides (e.g. CeO_2, Fe_xO_y, Al_xO_y, ZnO) and carbon nanotubes, ranging from 100 to 1000 t/year (Piccinno et al., 2012). This extensive use worldwide is causing increasing concern because of the potential release of NPs into the environment as single entities, as agglomerates or embedded in a matrix. Emission scenarios of NPs could occur during any stage of the their life cycle, i.e. production and manufacturing, use, and end-of-life management/disposal of NPs-containing products (Bundschuh et al., 2018), ending up into any of the environmental compartments (i.e. air, soil or water). NP release can occur directly from point (e.g. combustion processes, landfills, wastewater treatment plants, and factories) or non-point sources (e.g. from nanoproduct applications), as well as indirectly, such as from wet deposition after release from a point source into the atmosphere (Salieri et al., 2018). Since some NPs have proved toxic to cell cultures and human tissues, as well as to test organisms (Kumar et al., 2017; Madhwani, 2013), the scientific community is questioning the human and environmental risk resulting from the possible release of NPs from nano-based products. Upon reaching the aquatic environment, the fate and behavior of NPs is likely to be controlled by their intrinsic properties, such as size, shape, surface charge and, to a large extent, by environmental parameters, such as pH, ionic strength (IS), temperature, and presence and composition of natural organic matter (NOM), as well as by possible interaction with natural colloidal particles (NCPs) of different origin and composition. It

has been demonstrated that both NOM and NCPs would significantly affect NPs fate and behavior in surface waters (Clavier et al., 2019; Huang et al., 2018; Luo et al., 2018), especially given the higher order of magnitude of the concentration of these natural components with respect to NPs: generally, mg L^{-1} for NOM and NCPs while ng·L^{-1}-µg·L^{-1} for NPs (Baalousha et al., 2009).

One of the main processes influencing the behavior of NPs in an aquatic system is agglomeration, which generally leads to the formation of large structures, followed by particle sedimentation in the water body (Buffle et al., 1998). Aggregation is the result of homo- (interaction between particles of the same type) and heteroaggregation (aggregation between non-similar particles, e.g. NCPs and NPs), with the latter process generally dominating the overall fate of NPs under environmental conditions.

Up to now, numerous studies on NCPs-NPs heteroaggregation have been performed, either experimentally (Barton et al., 2014; Feng et al., 2019; Gallego-Urrea et al., 2016; Geitner et al., 2017; Quik et al., 2012; Slomberg et al., 2019; Smith et al., 2015) or by developing numerical/theoretical models (Künniger et al., 2014; Praetorius et al., 2012; Quik et al., 2014; Shen et al., 2014). The main challenge to accurately estimate NCPs-NPs heteroaggregation is the determination of the attachment efficiency (α), which defines the probability of a collision among particles or aggregates to end in an attachment. Depending on the aggregation stage studied, different α values can be estimated: the system specific α_{global} at long time scale (at equilibrium) or the individual α_{hetero} at the early stage of heteroaggregation (Praetorius et al., 2020). However, by applying both experimental and modeling approaches, the complexity of these multiple and very fast interactions among dispersed particles in surface waters makes the determination of α values still challenging, calling for additional efforts. Usually, the

experimental approaches proposed by many authors so far were based on investigating NPs fate and behavior in both artificial and natural surface waters, even with different NOM types in terms of chemical composition and molecular weight. However, studies focusing on the potential interactions between NPs and NCPs are still scarce and usually only a single type of inorganic NCPs, e.g. montmorillonite (Zhou et al., 2012), SiO_2 (Praetorius et al., 2014), illite (Adam et al., 2016; Gallego-Urrea et al., 2016) or kaolinite (Badetti et al., 2021) was tested.

In this work, the colloidal behavior of P25 TiO_2 NPs has been investigated both in artificial waters (i.e. deionized water, artificial fresh and marine waters) and in brackish water of the Venice lagoon (Italy), in the presence of kaolinite (with and without NOM addition) as well as of NCPs. Kaolinite was selected as a proxy for NCPs, while the latter were extracted from surface sediments of the lagoon by an ad-hoc developed procedure to obtain a particle size ranging from nano to micrometers. The experimental data, obtained by means of Dynamic and Electrophoretic Light Scattering (DLS and ELS) and Centrifugal Separation Analysis (CSA), were statistically analyzed by clustering techniques and integrated into a global stability index recently developed by our research group (Badetti et al., 2021) to rank different dispersions according to their colloidal stability.

The aim of this work was to understand whether: i) the global stability index (I_G) could be a robust statistical tool to quantitatively classify the colloidal stability of single- and multi-component colloidal dispersions under the different experimental conditions tested; ii) the outcomes from a clustering technique, without any *a priori* knowledge of the colloidal stability categorization of the different dispersions, would be consistent with the classification obtained by means of the global stability index; iii) kaolinite could

be a good surrogate for mimicking the colloidal behavior of NCPs.

2. Materials and methods

2.1 Aqueous media

Deionized water (DW, pH=7) was produced by a MilliQ® water purifier system (Millipore, Bedford, MA, USA, ≥ 18.2 MΩ·cm, TOC ≤ 3 ppb) and used as reference medium. Artificial Fresh Water (AFW, pH=7.5) and Artificial Marine Water (AMW, pH=8.5) were prepared according to OECD and ASTM standardized protocols (ASTM D1141-98 - Reapproved 2003. Standard Practice for the Preparation of Substitute Ocean Water, 2003; OECD Guidelines for Testing of Chemicals N° 203 - Fish Acute Toxicity Test - Annex 2 Composition of the recommended reconstituted water, 1992), with a calculated IS of 2 and 630 mM, respectively (water compositions are reported in Table S1). All inorganic salts were of analytical grade and purchased from Merck (Darmstadt, Germany).

Lagoon Water (LW, pH=8.5) from the lagoon of Venice (Italy) was collected in October 2019 at the San Giuliano sampling site (Figure 1, 45° 27' 46.2"N, 12° 17' 22.6"E), located within the central basin of the lagoon, close to rivers inflow and to the mainland. LW was stored in a dark brown glass bottle immediately after sampling, filtered through a 0.22 µm cellulose acetate membrane (47 mm diameter Merck MilliPore®, Darmstadt, Germany) and eventually frozen prior to use.

The rationale behind the selection of these four aqueous media was based on harmonized media recommendations by Geitner et al., 2020.

Ion-exchange chromatography (IEC, Dionex DX 320) was employed to determine ion concentration (Ca^{2+}, Mg^{2+}, Na^{+}, K^{+}, Cl^{-} SO_4^{2-}). in AFW, AMW and LW. The stationary phase

for the determination of anions consisted of an AS14 anionic column, preceded by an AG14 guard column. The mobile phase, in isocratic elution, was a 23 mM NaOH solution in DW, with 1.2 $mL \cdot min^{-1}$ flow and 100 mA current. The stationary phase for the determination of cations employed a CS12 cationic column, preceded by a CG12 guard column. The mobile phase, in isocratic elution, was a 22 mM H_2SO_4 solution in DW, with 1 $mL \cdot min^{-1}$ flow and 100 mA current.

Figure 1. Location map of the San Giuliano sampling site (45° 27' 46.2"N, 12° 17' 22.6"E) in the Venice lagoon (Italy, North-Est).

106 **2.2 TiO_2 NPs**

107 The inorganic titanium dioxide P25 nano-powder (TiO_2 NPs) was purchased from
108 PlasmaChem GmbH (Mainz, Germany) and stored in the dark at room temperature until
109 use. The TiO_2 NPs have an average particle size of 21 nm and are a mixture of approx.
110 80% anatase and 20% rutile (99.5% of purity), with a 50 ± 15 $m^2 \cdot g^{-1}$ surface area and a
111 bulk density of 3.8 $g \cdot cm^{-3}$. Primary characterization was already reported in our previous
112 works (Brunelli et al., 2016, 2013).

113

114 **2.3 Suwanee River natural organic matter**

115 Suwannee River Natural Organic Matter (SR-NOM, 2R101N) reference sample was
116 purchased from the International Humic Substances Society (IHSS, Atlanta, GA, USA),
117 with a total carbon content of around 40% (w/w) (International Humic Substances
118 Society, 2012). Since it is well characterized, standardized and extensively used by many
119 research groups worldwide, SR-NOM was chosen as a model for NOM of surface waters.
120 A stock dispersion of SR-NOM at 500 $mg \cdot L^{-1}$ was prepared, stirred over 24 h to ensure
121 complete dissolution and filtered by 0.45 µm filter membrane to remove the insoluble
122 materials.

123

124 **2.4 Kaolinite**

125 As a possible surrogate to represent NCPs in the water column, kaolinite powder was
126 purchased from The Clay Mineral Society (KGa-1b, low-defect, Warren County, Georgia,
127 USA). As reported by the manufacturer, it is mainly composed by SiO_2 (44.2%), and Al_2O_3
128 (39.7%), with low amounts of TiO_2 (1.4%), Fe_2O_3 (0.13%) and FeO (0.08%). The Cation
129 Exchange Capacity (CEC) is 2 meq 100 g^{-1} with a surface area of 10.05 ± 0.02 m^2 g^{-1} and

130 a density of approximately 2.60-2.65·10^3 kg m^{-3}. Before use, a pre-treatment of kaolinite
131 was performed to obtain a particles size range more similar to natural inorganic
132 particulate matter found in surface waters and to generate reproducible data (Zhang et
133 al., 2017). Briefly, according to Badetti et al., 2021 kaolinite was pre-treated by 10
134 washes with 1M NaCl, 5 washes with 1M NaOH, and 5 washes with deionized water.
135 After each washing step, the solid was recovered by centrifugation (Jouan CR3i
136 centrifuge, UK) at a Relative Centrifugal Force (RCF) of 8028 *g* for 10 min. After the final
137 centrifugation step, the treated kaolinite was dried overnight at 50 °C into a convection
138 oven and stored in the dark until analysis.
139 Morphological structure and chemical composition of kaolinite was investigated by
140 means of Scanning Electron Microscopy (Nova NanoSEM 450, FEI, Eindhoven, The
141 Netherlands) coupled with Energy Dispersive X-ray Spectrometry (Bruker Quantax-200
142 EDS, Bruker Nano GmbH, Berlin, Germany). The SEM images were analyzed by ImageJ
143 software v. 1.52a. The qualitative mineralogical information for kaolinite powder was
144 obtained by means of X-Ray Powder Diffraction (XRPD, X'Pert PRO XRDP, Malvern
145 Panalytical Ltd, United Kingdom).
146
147 **2.5. Natural colloidal particles extraction from sediment of the Venice lagoon**
148 Surface sediment (0-5 cm depth) was sampled by a manual corer at the same site where
149 LW was collected (Figure 1). This site was selected on the basis of the very high content
150 of the fine fraction (< 63 µm) in sediments (70-80% w/w, according to Facca et al., 2014),
151 suitable to obtain a reasonable amount of natural colloids from the extraction
152 procedure. The sample was first wet-sieved through a 2-mm sieve and then freeze-dried.
153 Afterwards, it was pulverized with an agate mortar and then dry-sieved through a 63 µm

sieve. The obtained fine fraction (<63 μm) was used to develop a method for the extraction of the natural colloidal particles (NCPs). NCPs powder was characterized by SEM-EDS and XRPD as described for kaolinite in paragraph 2.4.

Total and inorganic carbon content of dry NCPs was determined by the 1500 CNS Analyser (Carlo Erba). Organic carbon content was determined by difference.

2.6 Single- and multi-component dispersions preparation

The colloidal behavior of P25 (100 mg L^{-1}), kaolinite and NCPs (1 g L^{-1} for both) were investigated in the four aqueous media selected as single component as well as by mixing either kaolinite or NCPs with P25. According to the concentration ranges of TOC usually found in the different types of surface waters, also SR-NOM was opportunely added to the different dispersions as follows: 0.1 mg·L^{-1} in DW (as reference) and AMW, while 10 mg·L^{-1} in AFW. SR-NOM was not added to LW and to the dispersions containing NCPs, since they already naturally contain organic carbon (around 1% in NCPs, as measured by the CNS analyser). A summary of the dispersions investigated is displayed in Table 1. Each dispersion was probe sonicated in an ice bath at 100 W for 10 min (0.5 cycle 80% amplitude) before use.

Table 1. Overview of the single and multi-component dispersions matrix investigated (7 x 4 dispersions).

		DW	AFW	AMW	LW
Single component	TiO_2 NPs	1x	1x	1x	1x
	kaol	1x	1x	1x	1x
	kaol with NOM	1x	1x	1x	-
	NCPs	1x	1x	1x	1x
Multi component	TiO_2 NPs/kaol	1x	1x	1x	1x
	TiO_2 NPs/kaol with NOM	1x	1x	1x	-
	TiO_2 NPs/NCPs	1x	1x	1x	1x

2.7 Colloidal stability assessment of single- and multi-component dispersions

The colloidal stability of both single- and multi-component dispersions in DW, AFW, AMW and LW was investigated by means of Dynamic Light Scattering (DLS), Electrophoretic Light Scattering (ELS) and by Centrifugal Separation Analysis (CSA) after five minutes of probe sonication, delivering a power of 100 W for 5 min using a pulsed 80% mode.

DLS and ELS were performed by means of the multi-angle Nicomp ZLS Z3000 (Particle Sizing System, Port Richey, FL, USA). The intensity-based average hydrodynamic diameter, d_H, was measured with an optical fiber set at 90° scattering angle (W=25 mW and λ=639 nm) for 5 minutes to obtain a robust average statistic of the aggregate size. Surface charge of the electric double layer of each dispersion was determined by applying a 5 V electric field to obtain zeta-potential (ζ-pot) values, using the Smoluchowski approximation. All the measurements were performed in triplicate and

results of both d_H and ζ-pot are expressed as average.

Centrifugal separation analysis (CSA) by the Multiwavelength Dispersion Analyzer LUMiSizer® 651 (L.U.M. GmbH, Berlin, Germany) was carried out to estimate the sedimentation velocity (V-sed) of the dispersed phase in the different media selected. Transmission profiles were recorded every 5 seconds (41 minutes of runtime) at 470 nm, T=25°C, and rotation per minute (RPM)=2000, which corresponds to 537 relative centrifugal force (RCF) at 120 mm far from the rotor of the centrifuge. The linear dependency between RCF and V-sed already demonstrated in several works by our research group (Badetti et al., 2021; Brunelli et al., 2018, 2016) allowed to estimate V-sed data at gravity by dividing the sedimentation velocity values calculated by the instrument for the RCF applied. All the measurements were performed in triplicate and the results are expressed as median.

2.8 Clustering analysis

The experimental data obtained by the DLS, ELS and CSA techniques were statistically analyzed by unsupervised agglomerative hierarchical clustering to highlight potential groups of similarity without any *a priori* knowledge on data categorization. Clustering methods have been already used to classify nanomaterials into groups based on some similarities, e.g. regarding their influence on the biological activity (Cai et al., 2018; Shaw et al., 2008), gene expression (Ilves et al., 2019), mechanisms of action towards cells (Scala et al., 2018) and colloidal stability (Brunelli et al., 2018).

In this work, raw data were first autoscaled, by centering (subtracting the mean of each variable to each value) and scaling (dividing each value by the standard deviation of each variable). Thus, each of the three variables was transformed into a new variable with

the same weight (mean=0 and standard deviation=1). Euclidean distance matrix, based on the geometric distance between two points in the euclidean space, was calculated to determine the distance among samples. Then, by using the complete linkage method, which measures the distance between each cluster considering the longest distance from any member of one cluster to any member of the other cluster, was used.

2.9 Global stability index

According to a method recently developed by our research group (Badetti et al., 2021), in which the colloidal behavior of uncoated and polyvinylpyrrolidone (PVP) coated TiO_2 NPs was assessed in simulated aqueous media, the experimental data on the colloidal stability were mathematically combined to develop three relative indexes – one for each analytical technique employed (I_{DLS}, I_{ELS}, I_{CSA}) - by means of logistic curves and then merged into a global stability index (I_G) calculated as the average of I_{DLS}, I_{ELS} and I_{CSA} values (for further details see Badetti et al., 2021). The I_G values were then displayed by a heatmap, in which the increasing darkness of the color shade indicates higher stability.

3. Results and Discussion

3.1. Natural colloidal particles extraction from sediment of the Venice lagoon

The set up for the mechanical extraction of natural colloidal particles (NCPs) from sediment of the Venice lagoon, with size below 4 µm, was developed based on available methods reported in the literature. The most suitable extraction procedures to obtain NCPs were selected and are summarized and briefly described in Table S2. In general, after sample drying and sieving, these methods involve the resuspension of the solid sample in water, followed by agitation and/or mixing for a certain time, and then

centrifugation or sedimentation to isolate the desired particle fractions. The duration of the various steps varied according to the objectives of each study.

Based on the information summarized in Table S2 and of preliminary experiments with the sediment of the Venice lagoon aimed at testing different extraction conditions, the method developed to obtain NCPs below 4 µm is schematized in Figure 2. The optimized procedure involves different steps. After freeze-drying and sieving, the sediment fraction <63 µm (more than 90% as determined by weighing) is dispersed in DW at 1:10 (w/v) solid:liquid ratio, mixed for 1 h with a magnetic stirrer and allowed to settle for 30 min. The supernatant is then siphoned out and centrifuged at 6146 g for 15 min to ensure the complete precipitation of the particles, which are then dried overnight at 50 °C. The organic carbon content, determined by CNS analysis, was 0.8% (w/w).

The obtained NCPs were further characterized, together with standard kaolinite (prepared as described in paragraph 2.4), in order to compare the two materials.

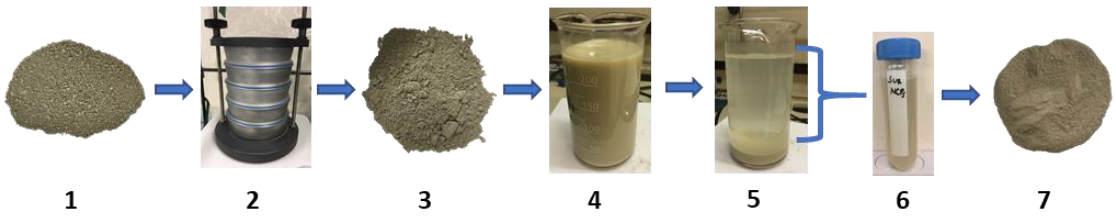

Figure 2. Scheme of the NCPs extraction procedure: 1) Freeze-drying of surface sediment; 2) Sieving up to < 63 µm; 3) NCPs powder with a particles size < 63 µm; 4) NCPs dispersion in DW, stirring for 1h; 5) Settling for 30 min, siphoning out of the supernatant; 6) Supernatant after centrifugation at 6146 g for 15 min; 7) Dried NCPs after centrifugation and oven drying.

263 **3.2 Shape, size and chemical composition of kaolinite and natural colloidal particles**

264 SEM analysis of kaolinite powder revealed the presence of quite regular agglomerates
265 of slightly squared shape (Figures 3 and S1). The length of the agglomerates ranged
266 between 2.7 and 6.5 µm, with an average of 4.0 ± 1.2 µm, and the width between 1.7
267 and 4.0 µm, with an average of 3.1 ± 0.7 µm.

268

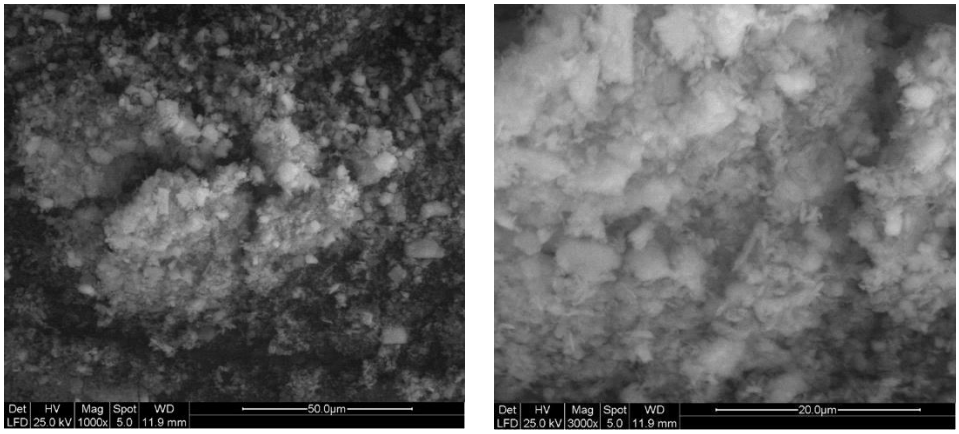

269

270 Figure 3. SEM micrographs of the kaolinite powder obtained at 1000x (left) and 3000x
271 (right) magnifications.

272

273 The elemental analysis performed by EDS probe (Figure S1) in different points and areas
274 of the kaolinite sample showed a good compositional homogeneity. The following
275 elements with their corresponding mole percentage were identified: O (74%), Al (12%)
276 and Si (12%) (Table S3).

277 In the case of NCPs extracted from the sediment of the Venice lagoon, SEM analysis
278 showed the presence of irregularly shaped agglomerates (Figures 4 and S2), with some
279 of them elongated and others more squared. The length of the agglomerates was
280 between 2.3 and 6.2 µm, with an average of 4.2 ± 1.3 µm, while the width was between

1.7 and 5.7 µm, with an average of 3.2 ± 1.3 µm.

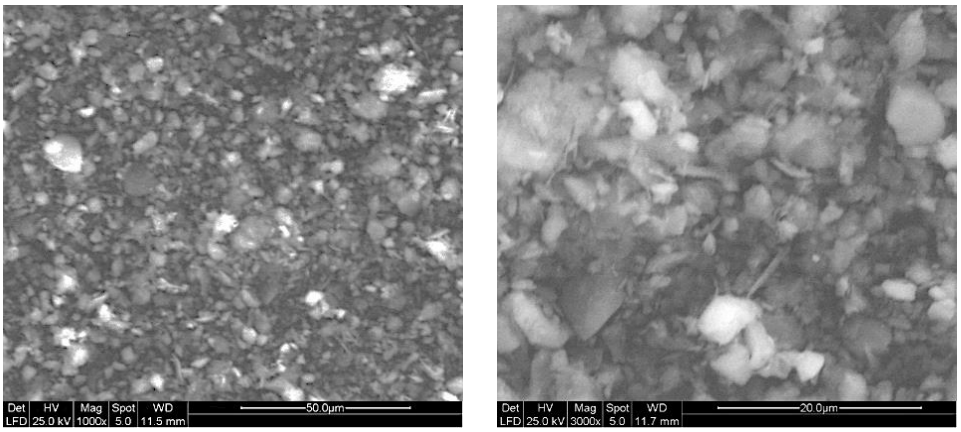

Figure 4. SEM micrographs of the NCPs sample obtained at 1000x (left) and 3000x (right) magnifications.

The EDS analysis of NCPs (Figure S2) showed a highly inhomogeneous sample, constituted by O (60%) and C (28%) as the main elements, and Mg, Al, Si, K, Ca, Fe with a minor content, ranging from 4.4 to 0.2% (moles percentage, Table S4).

Therefore, these analyses performed by SEM-EDS highlighted the more homogeneous shape and chemical composition of kaolinite agglomerates with respect to NCPs, with the latter showing higher complexity given by the natural origin. As far as particles size is concerned, no significant difference was observed between the two samples.

3.3. Mineralogical composition of kaolinite and natural colloidal particles

Figure 5 shows the X-Ray powder diffraction pattern of the kaolinite powder. The identification of the phases was performed by comparing the peak intensity positions with those from the international Centre for Diffraction Data. The diffractogram reveals

the presence of kaolinite as the main phase while anatase and quartz appear as minor phases.

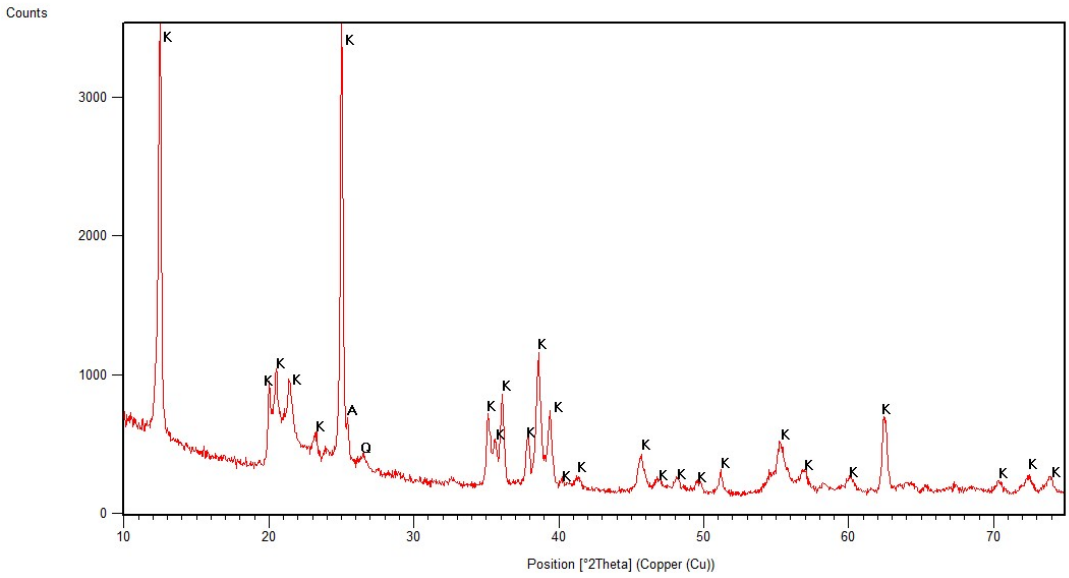

Figure 5. a) XRPD of kaolinite sample: K = kaolinite, A = anatase, Q = quartz.

The mineralogical analysis performed on NCPs sample by XRPD (Figure 6) allowed to identify the following crystalline phases, in a descending order based on the most characteristic peaks intensity: quartz [SiO_2], dolomite [$MgCa(CO_3)_2$], calcite [$CaCO_3$], and a mixed silicate of Al, Fe, K, Mg. The last phase does not have a well-defined stoichiometry due to the presence of impurities, even though a basic stoichiometry such as $Mg_2Al_4Si_5O_{18}$ could be hypothesized. The X-ray powder pattern obtained is typical of a fairly crystalline substance with a certain amorphous phase component (high background and quite wide peaks). The mineralogical composition obtained for NCPs is comparable to that reported in literature for sediments of the Venice lagoon (Hieke Merlin et al., 1979), in which silicates and carbonates (higher amount of dolomite with respect to calcite) are predominant.

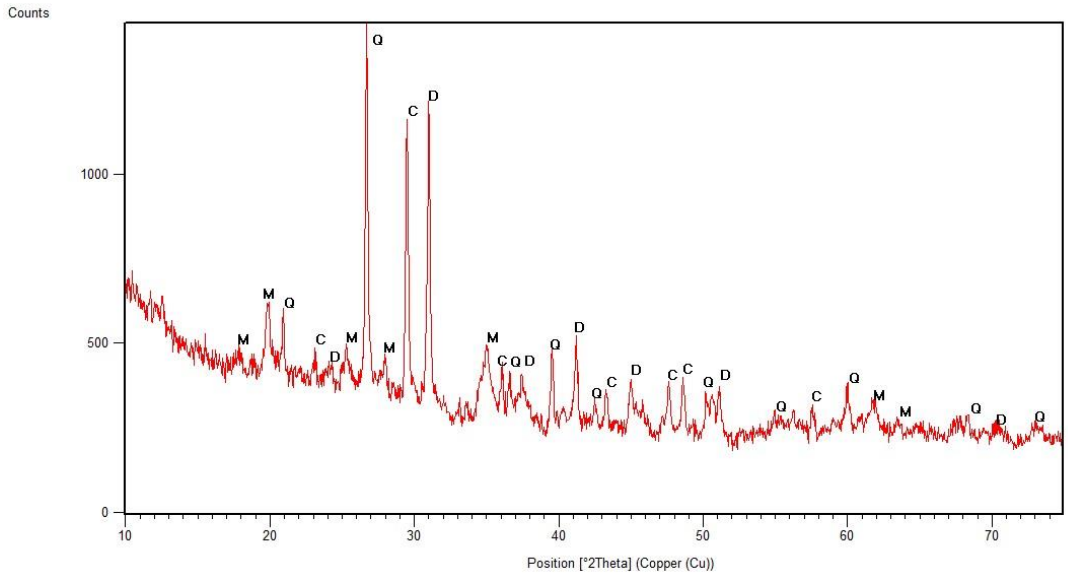

Figure 6. XRPD of NCPs sample: Q = quartz, D = dolomite, C = calcite, M = mixed silicate.

316

317 **3.4. Aqueous media characterization**

318 The ion concentrations in LW, AFW and AMW, determined by Ion-Exchange
319 Chromatography, are displayed in Table S5. The concentrations measured in LW were
320 13.24 ± 0.45 g/L for Cl^-, 1.60 ± 0.06 g/L for SO_4^{2-}, 7.29 ± 0.10 g/L for Na^+, 0.87 ± 0.01 g/L
321 for Mg^{2+}, 0.28 ± 0.04 g/L for K^+ and 0.16 ± 0.01 g/L for Ca^{2+}. As expected from the
322 common salinity values of brackish and marine waters, cations and ions concentration
323 found in the LW was slightly lower than AMW values.

324

325 **3.5 Colloidal characterization of single- and multi-component dispersions**

326 As already reported in literature (Ashraf et al., 2018; Brunelli et al., 2018; Loosli et al.,
327 2013), it is generally recognized that an increase of the hydrodynamic particles size in a
328 dispersion indicates agglomeration processes, followed by particle sedimentation if no
329 stabilizing components - e.g. natural organic matter (Chen and Elimelech, 2007) or
330 alginate (Callegaro et al., 2015; Dey et al., 2016; Pandey and Ramontja, 2016) - are

present. As far as zeta-potential is concerned, large positive or negative values (i.e. ±30 mV) commonly indicate a good dispersion stability due to electrostatic repulsion among particles, while the maximum colloidal instability of a dispersion is reached at a pH close to the point of zero charge (PZC) (Hunter, 1981). However, systematic studies of NPs' fate and behavior in water media mimicking environmental conditions could lead to different outcomes due to complex interactions between the NPs and their surroundings. To this end, the results of the colloidal characterization of single (P25, kaol, kaol/SR-NOM and NCPs) and multi-component (kaol/P25, kaol/SR-NOM/P25, NCPs/P25) dispersions in the different water media used in this study are summarized in Table 2 and discussed below.

Table 2. Hydrodynamic diameter (d_H), Sedimentation velocity (V-sed) and zeta potential (ζ-pot) of the tested single- and multi-component dispersions in DW (pH=7), AFW (pH=7.5), AMW (pH=8.5) and LW (pH=8.5) at 20 °C. Concentrations tested: 0.1 mg·L^{-1} SR-NOM$_{TOC}$ in DW and AMW; 10 mg·L^{-1} SR-NOM$_{TOC}$ in AFW; 1 g·L^{-1} kaolinite or NCPs; 100 mg·L^{-1} TiO_2 NPs.

Sample		d_H (nm)			
		DW	AFW	AMW	LW
Single-component	TiO_2 NPs	633 ± 103	1081 ± 201	1538 ± 463	1979 ± 374
	kaol	719 ± 147	1128 ± 232	1497 ± 255	1631 ± 321
	Kaol with NOM	560 ± 105	696 ± 137	2311 ± 494	-
	NCPs	721 ± 136	1154 ± 231	1491 ± 254	1566 ± 302
Multi-component	TiO_2 NPs/kaol	1372 ± 276	2011 ± 347	1852 ± 374	1869 ± 377
	TiO_2 NPs/kaol NOM	1778 ± 331	773 ± 220	2615 ± 454	-
	TiO_2 NPs/NCPs	1140 ± 224	1742 ± 294	1812 ± 368	2557 ± 503

Sample		V-sed (µm s^{-1})			
		DW	AFW	AMW	LW
Single-component	TiO_2 NPs	0.24 ± 0.01	0.33 ± 0.01	0.37 ± 0.01	0.36 ± 0.01
	kaol	0.23 ± 0.01	0.52 ± 0.01	0.49 ± 0.02	0.45 ± 0.02
	Kaol with NOM	0.20 ± 0.01	0.22 ± 0.01	0.46 ± 0.02	-
	NCPs	0.26 ± 0.01	0.33 ± 0.03	0.48 ± 0.02	0.48 ± 0.02
Multi-component	TiO_2 NPs/kaol	0.55 ± 0.01	0.50 ± 0.01	0.46 ± 0.01	0.46 ± 0.01
	TiO_2 NPs/kaol NOM	0.39 ± 0.04	0.17 ± 0.01	0.55 ± 0.06	-
	TiO_2 NPs/NCPs	0.23 ± 0.01	0.49 ± 0.01	0.50 ± 0.02	0.51 ± 0.04

Sample		ζ-pot (mV)			
		DW	AFW	AMW	LW
Single-component	TiO_2 NPs	20.4 ± 2.5	-4.8 ± 0.6	-7.9 ± 2.2	-6.9 ± 1.4
	kaol	-12.3 ± 2.8	-13.0 ± 2.8	-2.5 ± 0.4	-2.0 ± 0.7

	Kaol with NOM	-19.4 ± 2.8	-13.5 ± 2.3	-2.0 ± 4.9	-
	NCPs	-15.9 ± 0.7	-11.3 ± 0.5	-3.9 ± 0.6	-2.8 ± 1.2
Multi-component	TiO_2 NPs/kaol	-11.5 ± 1.7	-11.6 ± 1.1	-2.6 ± 1.5	-6.7 ± 1.9
	TiO_2 NPs/kaol NOM	-18.9 ± 3.0	-18.9 ± 1.0	-2.1 ± 1.6	-
	TiO_2 NPs/NCPs	-14.9 ± 0.4	-9.3 ± 0.8	-1.8 ± 0.6	-1.4 ± 0.5

Deionized water (DW) was selected as a reference medium, since it does not contain any ions, which usually interact with NPs influencing their colloidal stability (Baalousha et al., 2013). As can be observed from Table 2, P25 and kaolinite dispersed alone showed quite similar hydrodynamic diameter and sedimentation velocity values, but opposite ζ-pot sign (+20 vs -12 mV, respectively). These results show that both dispersions have a quite good colloidal stability in DW, even improved for kaolinite dispersion with SR-NOM. Moreover, the data obtained for NCPs extracted from the sediment of the Venice lagoon were in line with that of standard kaolinite. Moving from single- (i.e. kaolinite with and without SR-NOM, NCPs and P25) to multi-component dispersions (kaolinite or NCPs, mixed with P25), a significant increase to d_H values above 1100 nm was observed. In these mixtures, SR-NOM played a two-fold role: it induced a stabilization of kaolinite particles alone (d_H decreased from 719 to 560 nm) but a destabilization of the kaolinite/P25 mixture (d_H increased from 1372 to 1778 nm). As far as V-sed is concerned, multi-component dispersions with kaolinite showed higher values than the single-component ones, while the NCPs/P25 mixture exhibited the same behavior as NCPs alone. This could be ascribed to the presence of the organic carbon in NCPs (0.8 %) that helped to stabilize the particles in dispersion. This effect can also be observed in the ζ-pot values of the samples containing NCPs with respect to those containing kaolinite without SR-NOM.

Moving from DW to AFW, DLS data highlighted a slight increase of d_H for the single-component dispersions and a larger increase for the multi-component ones with respect to deionized water, indicating that agglomeration processes occurred in AFW, likely because of an increase of the IS of the dispersion medium. The addition of SR-NOM at a final TOC concentration of 10 mg/L (compared to 0.1 mg/L in DW) clearly helped in keeping average particle size low (< 800 nm) for both the single-and multi-component kaolinite systems. As far as ζ-pot values are concerned, a general decrease was observed moving from DW to AFW due to the increase of the medium IS. This finding was expected, since -, as already reported in the literature (Badetti et al., 2021; Naito et al., 2018; OECD, 2017; Ramirez et al., 2019)- ions, especially divalent ones such as Mg^{2+}, SO_4^{2-} or Ca^{2+}, are able to get adsorbed onto other particles' surface, changing the colloidal stability of a dispersion.

A small increase of sedimentation velocity values from DW to AFW was also observed, with the only exceptions of kaol/SR-NOM and kaol/SR-NOM/P25, for which SR-NOM induced a quite good dispersion stabilization. As far as the single-components in AFW are concerned, NCPs and P25 showed the lowest V-sed values (0.33 $\mu m \cdot s^{-1}$), while kaolinite showed a significantly higher value (0.52 $\mu m \cdot s^{-1}$). The quite low V-sed value of the NCPs dispersion could probably be due to the stabilization effect played by the organic matter naturally present in the sample.

Moving from AFW to AMW, pH and IS increased from 7 to 8.5 and from 2 to 630 mM, respectively. As can be observed from Table 2, the higher IS led to the formation of larger agglomerates for both the single and the multi-component dispersions, which reached d_H values also > 2000 nm. This last result could be ascribed to the potential interactions among the difference components studied, i.e. kaolinite, NCPs, P25, SR-NOM and free

ions, which favored the formation of larger structures. It has already been reported in the literature that NOM is able to form a coating around both TiO_2 NPs (with different composition and size) and kaolinite (Slomberg et al., 2019), and to increase the final colloidal stability of the dispersions at pH 8.5. However, it has been also observed that divalent electrolytes such as Ca^{2+}, Mg^{2+} and SO_4^{2-} are able to interact with the dispersed phase as well as with NOM, leading to the formation of macro-structures (Luo et al., 2018) which can agglomerate in different ways, depending on the media characteristics. With respect to DW and AFW, V-sed values showed a significant increase in AMW except for kaol and kaol/P25, with the lowest value (0.37 ± 0.01 $\mu m \cdot s^{-1}$) reached by P25 and similar higher values (in the range 0.48 - 0.55 $\mu m\ s^{-1}$) for the other dispersions tested, with and without SR-NOM. As far as ζ-pot is concerned, the highest value (-7.9 ± 2.2 mV) was recorded for P25 NPs alone, while the others shifted very close to 0 mV, highlighting the key role of IS in influencing ζ-pot values with respect to the pH and SR-NOM.

Despite the similar pH (8.5) and ionic composition of the AMW and LW media, it was expected to observe some differences in the colloidal stability of the tested dispersions in these two salty waters because of the higher organic carbon content still present in LW after filtration at 0.45 µm, which could induce a higher stabilization of suspended particles in the LW medium. However, the results in Table 2 highlighted almost always higher values of d_H in LW with respect to AMW, with the largest differences recorded by P25 (1538 nm vs 1979 nm) and NCPs/P25 (1812 nm vs 2557 nm), while similar values were obtained for V-sed (between 0.45 and 0.50 $\mu m\ s^{-1}$, except for 0.37 $\mu m\ s^{-1}$ for P25 alone in AMW) and ζ-pot (between -6.9 to -1.4 mV as average). Therefore, the organic carbon content in LW was probably not enough to limit the particles agglomeration.

3.6 Cluster analysis and global stability index

Statistical analysis on the new data matrix, obtained by autoscaling the raw data to have mean=0 and standard deviation=1, was performed by applying the agglomerative hierarchical clustering, using the complete linkage method. This method is based on the distance between their farthest members of the dataset, highlighting the differences between elements: it favors homogeneity between the elements of the cluster to the detriment of the clear differentiation between clusters. The resulted dendrogram is showed in Figure 7, with three different clusters identified following the elbow method (Figure S3). The main discriminant of this grouping was the medium composition (the cluster on the left included only dispersions with 0 or low IS, i.e. DW or AFW, while the cluster in the middle grouped only samples in salty waters) and, to lesser extent, the dispersed phase tested: except only for kaol dispersed in AFW, all the samples within the third cluster always included P25 as dispersed phase.

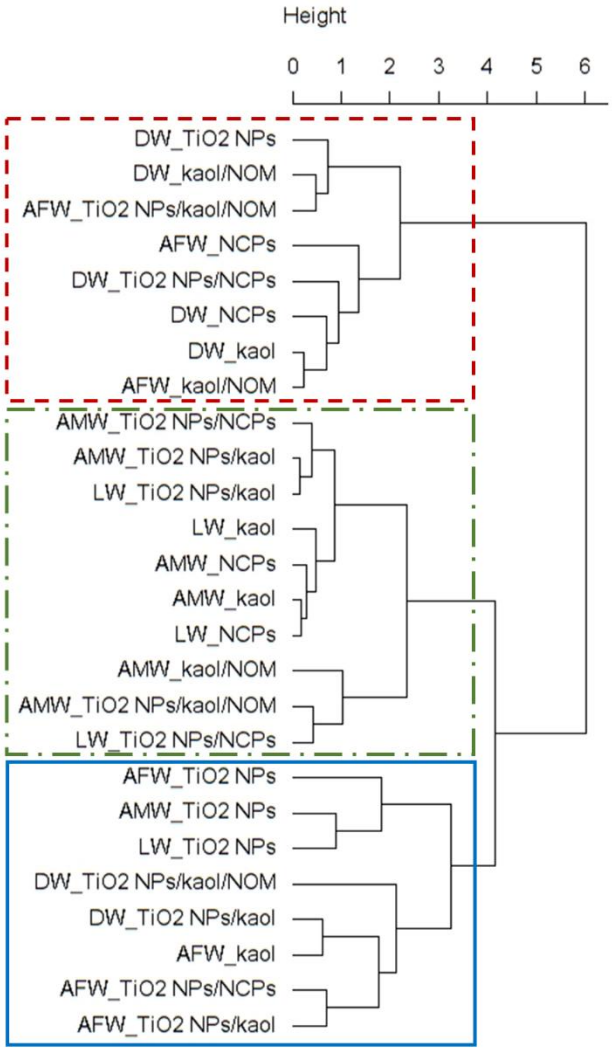

Figure 7. Hierarchical clustering analysis by using the complete linkage method. Three different clusters are differentiated by dashed, dashed-point and straight lines rectangles.

Besides clustering, the information acquired from DLS, ELS and CSA techniques was combined following a multi-method approach developed in a previous study (Badetti et al., 2021). Briefly, for each dispersion, three different technique-related indexes (I_{DLS}, I_{ELS} and I_{CSA}) were first calculated (Table S6) from hydrodynamic diameter, zeta-potential and sedimentation velocity data by means of the logistic curves reported in Badetti et

al., 2021. Then, the average of the values of the three indexes was calculated to finally obtain a global stability index (I_G) ranging from 0 to 1: the higher the I_G value, the more stable the dispersion. The overall I_G values obtained are reported in Table S6 and in Figure 8, in which the dispersions have been also grouped according to the three clusters identified and displayed in Figure 7. The graphical representation in Figure 8, which merges the information from the hierarchical clustering and the I_G approach, allows to classify the three different clusters based on the I_G values: the one on the top represents the high-stability cluster ($0.54 \leq I_G \leq 0.74$), the group on the bottom is the moderate-stability one ($0.42 \leq I_G \leq 0.53$) and the other in the middle refers to the low-stability cluster ($0.22 \leq I_G \leq 0.33$).

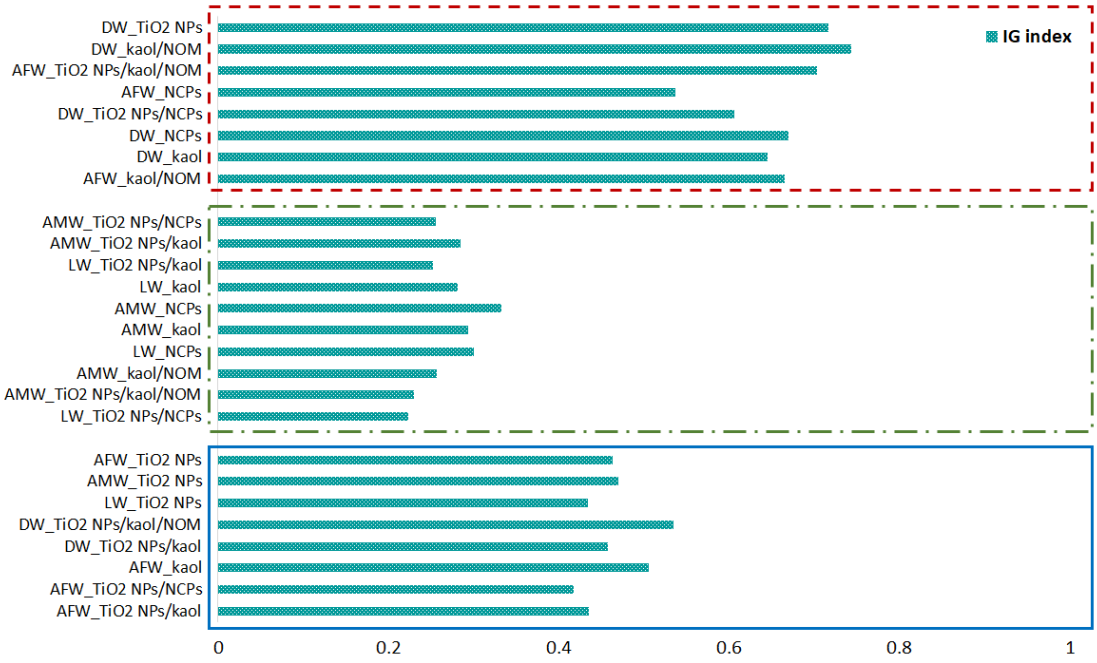

Figure 8. Global stability index (I_G) values. Each rectangle (with dashed, dashed-point and straight lines) represents one of the three clusters identified by the hierarchical clustering method used.

Furthermore, the overall I_G values have been displayed through the heatmap in Figure

449 9, allowing to quickly visualize the differences in colloidal stability by a continuous
450 gradation color. In general, the heatmap better highlights an increase in the colloidal
451 instability of the systems moving from low ionic strength media (DW and AFW) to salty
452 waters (AMW and LW). In detail, values for NCPs and kaol as single-component
453 dispersions were very similar in all the tested aqueous media, suggesting that, under the
454 conditions investigated in this work, kaolinite could represent a good analogue for
455 mimicking the behavior of natural colloids. Comparing the values of these single-
456 component (NCPs and kaol) with the corresponding NCPs/P25 or kaol/P25 multi-
457 component dispersions, quite similar I_G values were obtained in salty waters, while
458 slightly higher values (and therefore a higher stability) were observed in DW and AFW
459 for the single-component ones. This result could suggest that ions, especially the
460 divalent ones, are the main driving force of the behavior of dispersed particles in the
461 investigated aqueous media. As far as the dispersions with SR-NOM are concerned, i.e.
462 kaol/SR-NOM/P25 and kaol/SR-NOM, the high organic matter content (10 $mg \cdot L^{-1}$) added
463 to AFW likely formed a coating around P25 or kaolinite particles, stabilizing them against
464 aggregation (I_G values > 0.66). This stabilization effect was also observed in DW for
465 kaol/SR-NOM (I_G=0.74) and at a slightly lesser extent in kaol/SR-NOM/P25. Finally, the
466 role of SR-NOM in AMW was negligible (I_G values around 0.2) due to both the low SR-
467 NOM content added (0.1 $mg \cdot L^{-1}$) and to the very high concentration of ions, which
468 usually promote aggregation via bridging mechanisms (Loosli et al., 2014).
469
470

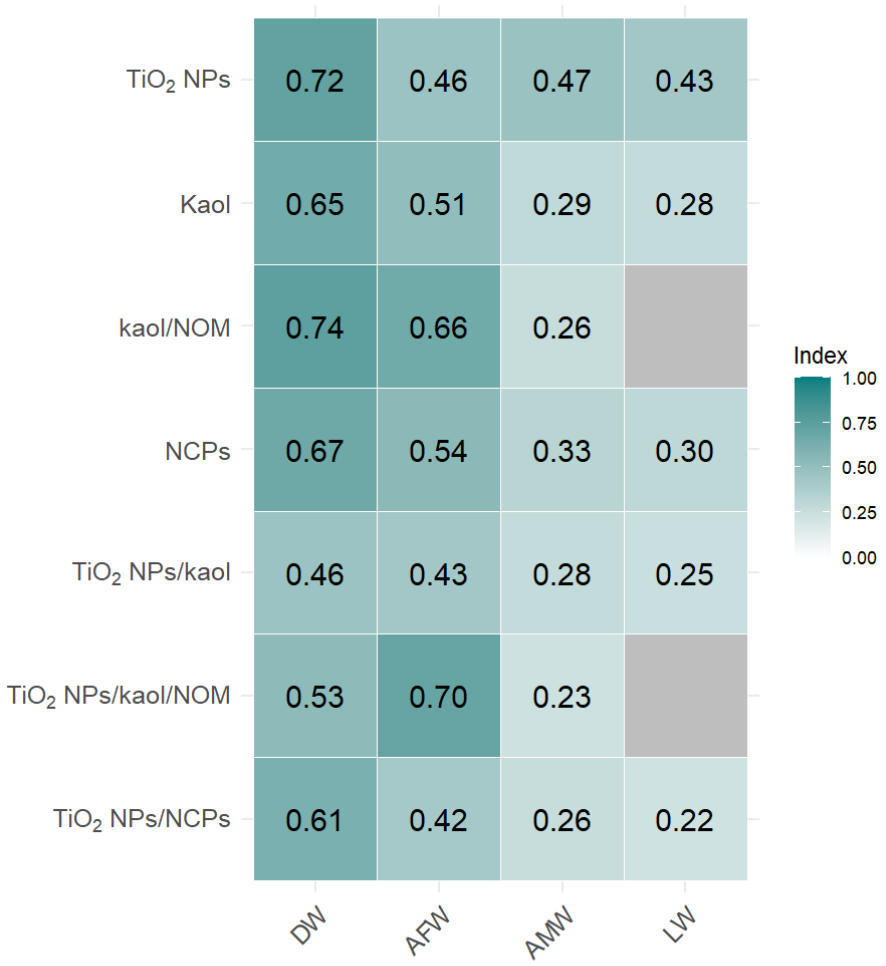

471

472 Figure 9. Heatmap of the I_G values of the different dispersed phases investigated. The
473 increasing darkness of the color shade indicates an increase of the dispersion stability.
474 The two missing I_G values correspond to the multi-component dispersions in LW, in
475 which SR-NOM was not added because LW has already a natural organic component.

476

477

4. Conclusions

Although in the last decade several studies on fate and behavior of engineered nanoparticles in simulated natural surface waters were published, there is still a need to increase knowledge on how these materials behave in the real aquatic environment.

The colloidal behavior of P25 TiO_2 NPs was investigated in artificial aqueous media with increasing ionic strength and natural organic matter content as well as in brackish water collected in the Venice lagoon. The multimethod approach applied, combining experimental data with the hierarchical clustering tool and the global stability index, demonstrated that: i) it is possible to quantitatively classify the colloidal stability of single- and multi-component colloidal dispersions in complex aqueous media; ii) the outcomes from the hierarchical clustering, without any *a priori* knowledge of the colloidal stability categorization of the different dispersions, is consistent with the colloidal stability ranking obtained through the global stability index; iii) kaolinite could be a good surrogate for NCPs to estimate the colloidal behavior of P25 TiO_2 NPs in natural aqueous media. Moreover, our findings suggest that the very high colloidal instability of the P25 TiO_2 NPs/NCPs mixture in the Venice lagoon water could lead to a higher exposure for benthic animals with respect to pelagic organisms. This could have important implications in assessing exposure, effect and ultimately risk of the P25 TiO_2 NPs in transitional environments.

Acknowledgments

Scientific activity performed in the Research Programme Venezia2021, coordinated by CORILA, with the contribution of the Provveditorato for the Public Works of Veneto, Trentino Alto Adige e Friuli Venezia Giulia.

References

Adam, V., Loyaux-Lawniczak, S., Labille, J., Galindo, C., del Nero, M., Gangloff, S., Weber, T., Quaranta, G., 2016. Aggregation behaviour of TiO<inf>2</inf> nanoparticles in natural river water. J. Nanoparticle Res. 18. https://doi.org/10.1007/s11051-015-3319-4

Ashraf, M.A., Peng, W., Zare, Y., Rhee, K.Y., 2018. Effects of Size and Aggregation/Agglomeration of Nanoparticles on the Interfacial/Interphase Properties and Tensile Strength of Polymer Nanocomposites. Nanoscale Res. Lett. 13, 214. https://doi.org/10.1186/s11671-018-2624-0

ASTM D1141-98 - Reapproved 2003. Standard Practice for the Preparation of Substitute Ocean Water, 2003. ASTM D1141-98, Standard Practice for the Preparation of Substitute Ocean Water, Re-approved.

Baalousha, M., Lead, J.R., von der Kammer, F., Hofmann, T., 2009. Natural Colloids and Nanoparticles in Aquatic and Terrestrial Environments, in: Environmental and Human Health Impacts of Nanotechnology. John Wiley & Sons, Ltd, pp. 109–161. https://doi.org/10.1002/9781444307504.ch4

Baalousha, M., Nur, Y., Römer, I., Tejamaya, M., Lead, J.R., 2013. Effect of monovalent and divalent cations, anions and fulvic acid on aggregation of citrate-coated silver nanoparticles. Sci. Total Environ. 454–455, 119–131. https://doi.org/https://doi.org/10.1016/j.scitotenv.2013.02.093

Badetti, E., Brunelli, A., Basei, G., Gallego-Urrea, J.A., Stoll, S., Walch, H., Praetorius, A., von der Kammer, F., Marcomini, A., 2021. Novel multimethod approach for the determination of the colloidal stability of nanomaterials in complex environmental mixtures using a global stability index: TiO2 as case study. Sci. Total Environ. 801,

149607. https://doi.org/https://doi.org/10.1016/j.scitotenv.2021.149607

Barton, L.E., Therezien, M., Auffan, M., Bottero, J.-Y., Wiesner, M.R., 2014. Theory and Methodology for Determining Nanoparticle Affinity for Heteroaggregation in Environmental Matrices Using Batch Measurements. Environ. Eng. Sci. 31, 421–427. https://doi.org/10.1089/ees.2013.0472

Brunelli, A., Badetti, E., Basei, G., Izzo, F.C., Hristozov, D., Marcomini, A., 2018. Effects of organic modifiers on the colloidal stability of TiO2 nanoparticles. A methodological approach for NPs categorization by multivariate statistical analysis. NanoImpact 9, 114–123. https://doi.org/https://doi.org/10.1016/j.impact.2018.03.001

Brunelli, A., Pojana, G., Callegaro, S., Marcomini, A., 2013. Agglomeration and sedimentation of titanium dioxide nanoparticles (n-TiO2) in synthetic and real waters. J. Nanoparticle Res. 15. https://doi.org/10.1007/s11051-013-1684-4

Brunelli, A., Zabeo, A., Semenzin, E., Hristozov, D., Marcomini, A., 2016. Extrapolated long-term stability of titanium dioxide nanoparticles and multi-walled carbon nanotubes in artificial freshwater. J. Nanoparticle Res. 18, 113. https://doi.org/10.1007/s11051-016-3412-3

Buffle, J., Wilkinson, K.J., Stoll, S., Filella, M., Zhang, J., 1998. A Generalized Description of Aquatic Colloidal Interactions: The Three-colloidal Component Approach. Environ. Sci. Technol. 32, 2887–2899. https://doi.org/10.1021/es980217h

Bundschuh, M., Filser, J., Lüderwald, S., McKee, M.S., Metreveli, G., Schaumann, G.E., Schulz, R., Wagner, S., 2018. Nanoparticles in the environment: where do we come from, where do we go to? Environ. Sci. Eur. 30, 6. https://doi.org/10.1186/s12302-018-0132-6

Cai, X., Dong, J., Liu, J., Zheng, H., Kaweeteerawat, C., Wang, F., Ji, Z., Li, R., 2018. Multi-

550 hierarchical profiling the structure-activity relationships of engineered
551 nanomaterials at nano-bio interfaces. Nat. Commun. 9, 4416.
552 https://doi.org/10.1038/s41467-018-06869-9
553 Callegaro, S., Minetto, D., Pojana, G., Bilanicová, D., Libralato, G., Volpi Ghirardini, A.,
554 Hassellöv, M., Marcomini, A., 2015. Effects of alginate on stability and ecotoxicity
555 of nano-TiO2 in artificial seawater. Ecotoxicol. Environ. Saf. 117, 107–114.
556 https://doi.org/https://doi.org/10.1016/j.ecoenv.2015.03.030
557 Chen, K.L., Elimelech, M., 2007. Influence of humic acid on the aggregation kinetics of
558 fullerene (C60) nanoparticles in monovalent and divalent electrolyte solutions. J.
559 Colloid Interface Sci. 309, 126–134. https://doi.org/10.1016/j.jcis.2007.01.074
560 Clavier, A., Praetorius, A., Stoll, S., 2019. Determination of nanoparticle
561 heteroaggregation attachment efficiencies and rates in presence of natural organic
562 matter monomers. Monte Carlo modelling. Sci. Total Environ. 650, 530–540.
563 https://doi.org/10.1016/j.scitotenv.2018.09.017
564 Dey, S., Sherly, M.C.D., Rekha, M.R., Sreenivasan, K., 2016. Alginate stabilized gold
565 nanoparticle as multidrug carrier: Evaluation of cellular interactions and hemolytic
566 potential. Carbohydr. Polym. 136, 71–80.
567 https://doi.org/https://doi.org/10.1016/j.carbpol.2015.09.016
568 DTU Environment, 2017. The Nanodatabase, [WWW Document]. URL
569 http://nanodb.dk/en/
570 Facca, C., Ceoldo, S., Pellegrino, N., Sfriso, A., 2014. Natural Recovery and Planned
571 Intervention in Coastal Wetlands: Venice Lagoon (Northern Adriatic Sea, Italy) as a
572 Case Study. Sci. World J. 2014, 968618. https://doi.org/10.1155/2014/968618
573 Feng, Y., Huynh, K.A., Xie, Z., Liu, G., Gao, S., 2019. Heteroaggregation and sedimentation

574 of graphene oxide with hematite colloids: Influence of water constituents and
575 impact on tetracycline adsorption. Sci. Total Environ. 647, 708–715.
576 https://doi.org/https://doi.org/10.1016/j.scitotenv.2018.08.046
577 Gallego-Urrea, J.A., Hammes, J., Cornelis, G., Hassellöv, M., 2016. Coagulation and
578 sedimentation of gold nanoparticles and illite in model natural waters: Influence of
579 initial particle concentration. NanoImpact 3–4, 67–74.
580 https://doi.org/https://doi.org/10.1016/j.impact.2016.10.004
581 Geitner, N.K., O'Brien, N.J., Turner, A.A., Cummins, E.J., Wiesner, M.R., 2017. Measuring
582 Nanoparticle Attachment Efficiency in Complex Systems. Environ. Sci. Technol. 51,
583 13288–13294. https://doi.org/10.1021/acs.est.7b04612
584 Geitner, N.K., Ogilvie Hendren, C., Cornelis, G., Kaegi, R., Lead, J.R., Lowry, G. V, Lynch,
585 I., Nowack, B., Petersen, E., Bernhardt, E., Brown, S., Chen, W., de Garidel-Thoron,
586 C., Hanson, J., Harper, S., Jones, K., von der Kammer, F., Kennedy, A., Kidd, J.,
587 Matson, C., Metcalfe, C.D., Pedersen, J., Peijnenburg, W.J.G.M., Quik, J.T.K.,
588 Rodrigues, S.M., Rose, J., Sayre, P., Simonin, M., Svendsen, C., Tanguay, R., Tefenkji,
589 N., van Teunenbroek, T., Thies, G., Tian, Y., Rice, J., Turner, A., Liu, J., Unrine, J.,
590 Vance, M., White, J.C., Wiesner, M.R., 2020. Harmonizing across environmental
591 nanomaterial testing media for increased comparability of nanomaterial datasets.
592 Environ. Sci. Nano 7, 13–36. https://doi.org/10.1039/C9EN00448C
593 Hieke Merlin, O., Menegazzo Vitturi, L., Semenzato, G., 1979. Contributo alla conoscenza
594 dei sedimenti superficiali della Laguna Veneta. Atti Istituto Veneto Scienze, Lettere
595 e Arti, Classe Sc.F.M.N., pp. 35–51.
596 Huang, G., Li, X., Lou, L., Hua, Y., Zhu, G., Li, M., Zhang, H.T., Xiao, J., Wen, B., Yue, M.,
597 Zhang, X., 2018. Engineering Bulk, Layered, Multicomponent Nanostructures with

598 High Energy Density. Small 14. https://doi.org/10.1002/smll.201800619
599 Hunter, R.J., 1981. Colloid Science, in: HUNTER, R.J. (Ed.), Zeta Potential in Colloid
600 Science. Academic Press, p. ii. https://doi.org/https://doi.org/10.1016/B978-0-12-
601 361961-7.50001-8
602 Ilves, M., Kinaret, P.A.S., Ndika, J., Karisola, P., Marwah, V., Fortino, V., Fedutik, Y.,
603 Correia, M., Ehrlich, N., Loeschner, K., Besinis, A., Vassallo, J., Handy, R.D., Wolff,
604 H., Savolainen, K., Greco, D., Alenius, H., 2019. Surface PEGylation suppresses
605 pulmonary effects of CuO in allergen-induced lung inflammation. Part. Fibre
606 Toxicol. 16, 28. https://doi.org/10.1186/s12989-019-0309-1
607 International Humic Substances Society, 2012. Replenishment of the Reference
608 Suwannee River Natural Organic Matter [WWW Document]. URL
609 https://ecos.fws.gov/ServCat/DownloadFile/27023?Reference=28178 (accessed
610 1.26.21).
611 Kumar, V., Sharma, N., Maitra, S.S., 2017. In vitro and in vivo toxicity assessment of
612 nanoparticles. Int. Nano Lett. 7, 243–256. https://doi.org/10.1007/s40089-017-
613 0221-3
614 Künniger, T., Gerecke, A.C., Ulrich, A., Huch, A., Vonbank, R., Heeb, M., Wichser, A.,
615 Haag, R., Kunz, P., Faller, M., 2014. Release and environmental impact of silver
616 nanoparticles and conventional organic biocides from coated wooden façades.
617 Environ. Pollut. 184, 464–471.
618 https://doi.org/https://doi.org/10.1016/j.envpol.2013.09.030
619 Loosli, F., Le Coustumer, P., Stoll, S., 2014. Effect of natural organic matter on the
620 disagglomeration of manufactured TiO2 nanoparticles. Environ. Sci. Nano 1, 154–
621 160. https://doi.org/10.1039/C3EN00061C

622 Loosli, F., Le Coustumer, P., Stoll, S., 2013. TiO2 nanoparticles aggregation and
623 disaggregation in presence of alginate and Suwannee River humic acids. pH and
624 concentration effects on nanoparticle stability. Water Res. 47, 6052–6063.
625 https://doi.org/10.1016/j.watres.2013.07.021
626 Luo, M., Huang, Y., Zhu, M., Tang, Y., Ren, T., Ren, J., Wang, H., Li, F., 2018. Properties of
627 different natural organic matter influence the adsorption and aggregation behavior
628 of TiO2 nanoparticles. J. Saudi Chem. Soc. 22, 146–154.
629 https://doi.org/https://doi.org/10.1016/j.jscs.2016.01.007
630 Madhwani, K.P., 2013. Safe development of nanotechnology: A global challenge. Indian
631 J. Occup. Environ. Med. 17, 87–88. https://doi.org/10.4103/0019-5278.130833
632 Naito, M., Yokoyama, T., Hosokawa, K., Nogi, K.B.T.-N.T.H. (Third E. (Eds.), 2018. Chapter
633 3 - Characteristics and Behavior of Nanoparticles and Its Dispersion Systems.
634 Elsevier, pp. 109–168. https://doi.org/https://doi.org/10.1016/B978-0-444-64110-
635 6.00003-2
636 OECD, 2017. OECD Guideline for the Testing of Chemicals 318 - Dispersion Stability of
637 Nanomaterials in Simulated Environmental Media.
638 OECD Guidelines for Testing of Chemicals N° 203 - Fish Acute Toxicity Test - Annex 2
639 Composition of the recommended reconstituted water, 1992. OECD Guidelines for
640 Testing of Chemicals No. 203. Fish, Acute Toxicity Test - Annex 2 Composition of
641 the recommended reconstituted water.
642 Pandey, S., Ramontja, J., 2016. Sodium alginate stabilized silver nanoparticles-silica
643 nanohybrid and their antibacterial characteristics. Int. J. Biol. Macromol. 93, 712–
644 723. https://doi.org/10.1016/j.ijbiomac.2016.09.033
645 Piccinno, F., Gottschalk, F., Seeger, S., Nowack, B., 2012. Industrial production quantities

and uses of ten engineered nanomaterials in Europe and the world. J. Nanoparticle Res. 14, 1109. https://doi.org/10.1007/s11051-012-1109-9

Praetorius, A., Badetti, E., Brunelli, A., Clavier, A., Gallego-Urrea, J.A., Gondikas, A., Hassellöv, M., Hofmann, T., Mackevica, A., Marcomini, A., Peijnenburg, W., Quik, J.T.K., Seijo, M., Stoll, S., Tepe, N., Walch, H., von der Kammer, F., 2020. Strategies for determining heteroaggregation attachment efficiencies of engineered nanoparticles in aquatic environments. Environ. Sci. Nano. https://doi.org/10.1039/C9EN01016E

Praetorius, A., Labille, J., Scheringer, M., Thill, A., Hungerbühler, K., Bottero, J.-Y., 2014. Heteroaggregation of titanium dioxide nanoparticles with model natural colloids under environmentally relevant conditions. Environ. Sci. Technol. 48, 10690–10698. https://doi.org/10.1021/es501655v

Praetorius, A., Scheringer, M., Hungerbühler, K., 2012. Development of Environmental Fate Models for Engineered Nanoparticles—A Case Study of TiO2 Nanoparticles in the Rhine River. Environ. Sci. Technol. 46, 6705–6713. https://doi.org/10.1021/es204530n

Quik, J.T.K., Stuart, M.C., Wouterse, M., Peijnenburg, W., Hendriks, A.J., van de Meent, D., 2012. Natural colloids are the dominant factor in the sedimentation of nanoparticles. Environ. Toxicol. Chem. 31, 1019–1022. https://doi.org/10.1002/etc.1783

Quik, J.T.K., Velzeboer, I., Wouterse, M., Koelmans, A.A., van de Meent, D., 2014. Heteroaggregation and sedimentation rates for nanomaterials in natural waters. Water Res. 48, 269–279. https://doi.org/10.1016/j.watres.2013.09.036

Ramirez, L., Ramseier Gentile, S., Zimmermann, S., Stoll, S., 2019. Behavior of TiO2 and

CeO2 Nanoparticles and Polystyrene Nanoplastics in Bottled Mineral, Drinking and Lake Geneva Waters. Impact of Water Hardness and Natural Organic Matter on Nanoparticle Surface Properties and Aggregation. Water 11. https://doi.org/10.3390/w11040721

Salieri, B., Turner, D.A., Nowack, B., Hischier, R., 2018. Life cycle assessment of manufactured nanomaterials: Where are we? NanoImpact 10, 108–120. https://doi.org/https://doi.org/10.1016/j.impact.2017.12.003

Scala, G., Kinaret, P., Marwah, V., Sund, J., Fortino, V., Greco, D., 2018. Multi-omics analysis of ten carbon nanomaterials effects highlights cell type specific patterns of molecular regulation and adaptation. NanoImpact 11, 99–108. https://doi.org/https://doi.org/10.1016/j.impact.2018.05.003

Shaw, S.Y., Westly, E.C., Pittet, M.J., Subramanian, A., Schreiber, S.L., Weissleder, R., 2008. Perturbational profiling of nanomaterial biologic activity. Proc. Natl. Acad. Sci. 105, 7387–7392. https://doi.org/10.1073/pnas.0802878105

Shen, C., Wu, L., Zhang, S., Ye, H., Li, B., Huang, Y., 2014. Heteroaggregation of microparticles with nanoparticles changes the chemical reversibility of the microparticles' attachment to planar surfaces. J. Colloid Interface Sci. 421, 103–113. https://doi.org/https://doi.org/10.1016/j.jcis.2014.01.033

Slomberg, D.L., Ollivier, P., Miche, H., Angeletti, B., Bruchet, A., Philibert, M., Brant, J., Labille, J., 2019. Nanoparticle stability in lake water shaped by natural organic matter properties and presence of particulate matter. Sci. Total Environ. 656, 338–346. https://doi.org/10.1016/j.scitotenv.2018.11.279

Smith, B.M., Pike, D.J., Kelly, M.O., Nason, J.A., 2015. Quantification of Heteroaggregation between Citrate-Stabilized Gold Nanoparticles and Hematite

694 Colloids. Environ. Sci. Technol. 49, 12789–12797.
695 https://doi.org/10.1021/acs.est.5b03486
696 von der Kammer, F., Ottofuelling, S., Hofmann, T., 2010. Assessment of the physico-
697 chemical behavior of titanium dioxide nanoparticles in aquatic environments using
698 multi-dimensional parameter testing. Environ. Pollut. 158, 3472–3481.
699 https://doi.org/https://doi.org/10.1016/j.envpol.2010.05.007
700 Zhang, X., Stavn, R.H., Falster, A.U., Rick, J.J., Gray, D., Gould, R.W., 2017. Size
701 distributions of coastal ocean suspended particulate inorganic matter: Amorphous
702 silica and clay minerals and their dynamics. Estuar. Coast. Shelf Sci. 189, 243–251.
703 https://doi.org/https://doi.org/10.1016/j.ecss.2017.03.025
704 Zhou, D., Abdel-Fattah, A.I., Keller, A.A., 2012. Clay Particles Destabilize Engineered
705 Nanoparticles in Aqueous Environments. Environ. Sci. Technol. 46, 7520–7526.
706 https://doi.org/10.1021/es3004427
707